

Unified optical-model approach to low-energy antiproton annihilation on nuclei and to antiprotonic atoms

C.J. Batty^a, E. Friedman^b, A. Gal^b

^aRutherford Appleton Laboratory, Chilton, Didcot, Oxon OX11 0QX, UK

^bRacah Institute of Physics, The Hebrew University, Jerusalem 91904, Israel

Abstract

A successful unified description of \bar{p} nuclear interactions near $E = 0$ is achieved using a \bar{p} optical potential within a folding model, $V_{\text{opt}} \sim \bar{v} * \rho$, where a $\bar{p}p$ potential \bar{v} is folded with the nuclear density ρ . The potential \bar{v} fits very well the measured $\bar{p}p$ annihilation cross sections at low energies ($p_L < 200$ MeV/c) and the $1s$ and $2p$ spin-averaged level shifts and widths for the $\bar{p}\text{H}$ atom. The density-folded optical potential V_{opt} reproduces satisfactorily the strong-interaction level shifts and widths over the entire periodic table, for $A > 10$, as well as the few low energy \bar{p} annihilation cross sections measured on Ne. Both \bar{v} and V_{opt} are found to be highly absorptive, which leads to a saturation of reaction cross sections in hydrogen and on nuclei. Predictions are made for \bar{p} annihilation cross sections over the entire periodic table at these very low energies and the systematics of the calculated cross sections as function of A , Z and E is discussed and explained in terms of a Coulomb-modified strong-absorption model. Finally, optical potentials which fit simultaneously low-energy $\bar{p}-{}^4\text{He}$ observables for $E < 0$ as well as for $E > 0$ are used to assess the reliability of extracting Coulomb modified \bar{p} nuclear scattering lengths directly from the data. The relationship between different kinds of scattering lengths is discussed and previously published systematics of the \bar{p} nuclear scattering lengths is updated.

PACS: 24.10.Ht, 25.43.+t, 25.60.Dz

Keywords: Antiproton annihilation; Low energies; Optical potentials; Saturation; Antiprotonic atoms.

Corresponding author: E. Friedman

Tel: +972 2 658 4667, Fax: +972 2 658 6347,

E mail: elifried@vms.huji.ac.il

(October 24, 2018)

I. INTRODUCTION

The present paper is motivated by the recent publications of experimental annihilation cross sections for antiprotons on several targets at very low energies ($p_L < 100$ MeV/c) [1–3]. Some unexpected features observed in the dependence of these cross sections on the mass (A) and charge (Z) numbers have been very recently explained by us [4] as arising from saturation of the \bar{p} annihilation cross sections due to the strong absorption that is characteristic of the \bar{p} -nucleus interaction. Using an optical model approach we have shown that the $E = 0$ borderline between \bar{p} atoms and the scattering regime can be crossed using the same \bar{p} -nucleus potential, i.e. one can get good fits to experimental results both for \bar{p} atoms and for low energy annihilation cross sections with the same potential, at least within a given mass region of the periodic table. Such potentials are strongly absorptive, which leads to a remarkable saturation of the total reaction cross section with increasing A . Strong absorption has very recently been shown [5,6] to lead also to saturation of the widths of \bar{p} atomic states and to the prediction of relatively narrow deeply bound \bar{p} atomic states. The close analogy between bound-state widths and total reaction cross sections is best demonstrated by observing the corresponding expressions, assuming for simplicity a Schrödinger-type equation. The width Γ of an atomic level is then given in terms of the optical potential V_{opt} by:

$$\frac{\Gamma}{2} = -\frac{\int \text{Im}V_{\text{opt}}(r)|\psi(\mathbf{r})|^2 d\mathbf{r}}{\int |\psi(\mathbf{r})|^2 d\mathbf{r}} . \quad (1)$$

Here $\psi(\mathbf{r})$ is the \bar{p} full atomic wavefunction. The corresponding expression for the total reaction cross section at positive energies is

$$\sigma_R = -\frac{2}{\hbar v} \int \text{Im}V_{\text{opt}}(r)|\psi(\mathbf{r})|^2 d\mathbf{r} . \quad (2)$$

Here $\psi(\mathbf{r})$ is the \bar{p} -nucleus elastic scattering wavefunction and v is the c.m. velocity. We note that these expressions involve no approximation.

In the present work we extend the earlier work by presenting a full analysis of the dependence of calculated annihilation cross sections on A , on Z and on the energy up to 16 MeV ($p_L = 175$ MeV). Beginning with the $\bar{p}p$ system, we show that the available experimental results, including the strong-interaction spin-averaged shift and widths of the $\bar{p}\text{H}$ atom, are very well accounted for by a potential approach. Moving over to \bar{p} -nuclear systems, we observe that the strong-interaction level shifts and widths in \bar{p} atoms are well reproduced for $A > 10$, over the entire periodic table, by folding the above $\bar{p}p$ potential \bar{v} with the nuclear density and renormalizing slightly its strength, to obtain a \bar{p} -nucleus optical potential. Using this density-folded optical potential V_{opt} , we study the systematics of the predicted cross sections over the entire periodic table and show it to result naturally from the absorptive properties of the interaction under conditions of Coulomb focussing. The optical potentials are then used to derive \bar{p} -nucleus s -wave scattering lengths. We study the A dependence of these scattering lengths and compare them with those extracted directly from the low-energy data using approximation methods [7].

The paper is organized as follows. In Section II we define the optical potential and the various scattering amplitudes which are used throughout the present work. Section

III deals with the $\bar{p}p$ system and in Section IV we discuss the \bar{p} interaction with nuclei. Section V is devoted to the \bar{p} - ${}^4\text{He}$ system which is used for closely examining the scattering length approximation and Section VI extends the discussion to heavier systems. The work is summarized and concluded in Section VII.

II. OPTICAL POTENTIALS AND SCATTERING AMPLITUDES

The interaction of low energy antiprotons with nuclei, as well as the interaction of antiprotons bound in an atomic system, is described in this work by the conventional ‘ $t\rho$ ’ potential [8]

$$2\mu V_{\text{opt}}(r) = -4\pi\left(1 + \frac{A-1}{A}\frac{\mu}{m}\right)b_0\rho(r) \quad , \quad (3)$$

where m is the nucleon mass, μ is the \bar{p} -nucleus reduced mass, b_0 is an ‘effective scattering length’ complex parameter obtained from fits to the data and $\rho(r)$ is the nuclear density distribution normalized to A . The density $\rho(r)$ may also include the effect of folding in a finite-range two-body interaction. The factor $(A-1)/A$ in Eq. (3) is usually omitted in large A atomic studies [8], as we do also here (Sect. IV), but is retained of course in the discussion of the $\bar{p}p$ system in Sect. III and the \bar{p} -He system in Sect. V.

It is customary to describe the interaction of bound hadrons with the nucleus by the Klein-Gordon (KG) equation of the form:

$$\left[\nabla^2 - 2\mu(B + V_{\text{opt}} + V_c) + (V_c + B)^2\right]\psi = 0 \quad (\hbar = c = 1) \quad , \quad (4)$$

where B is the complex binding energy and V_c is the finite-size Coulomb interaction of the hadron with the nucleus, including vacuum-polarization terms. Equation (4) assumes that V_{opt} behaves as a Lorentz scalar. The use of the KG equation for \bar{p} atoms is justified as long as spin effects are negligible and one is interested in $(2j+1)$ averaging. As we are interested in this work in crossing the $E=0$ borderline between the bound atomic system and the low energy scattering regime, we use the same wave equation also for positive energies, namely

$$\left[\nabla^2 + k^2 - (2\varepsilon_{\text{red}}^{(A)}V_c - V_c^2) - 2\mu V_{\text{opt}}\right]\psi = 0 \quad (\hbar = c = 1) \quad (5)$$

where k and $\varepsilon_{\text{red}}^{(A)}$ are the wave number and reduced energy respectively in the c.m. system, and $(\varepsilon_{\text{red}}^{(A)})^{-1} = E_{\bar{p}}^{-1} + E_A^{-1}$ in terms of the c.m. total energies for the projectile and target, respectively. Equation (5) is the Lorentz scalar version of the KG equation used in Ref. [9] for studying K^+ interaction with nuclei. Near $E = 0$ both equations yield practically the same numerical results. Furthermore, we have verified that using the Schrödinger equation instead of the KG equation leads to calculated reaction cross sections that differ by 0.5% or less.

The scattering amplitude due to the wave equation (5) can be written in the form [10]

$$f(\theta) = f^{(c)}(\theta) + e^{2i\sigma}f^{(sc)}(\theta) \quad , \quad (6)$$

where $f^{(c)}(\theta)$ is the point Coulomb scattering amplitude,

$$f^{(c)}(\theta) = \frac{1}{k} \sum (2l+1) C_l^{(c)} P_l(\cos\theta) \quad , \quad C_l^{(c)} = e^{i\sigma_l} \sin\sigma_l \quad , \quad (7)$$

and with non-relativistic Coulomb phase shifts given by

$$\sigma_l = \arg\Gamma(1 + l - i\eta) \quad , \quad \eta = \frac{1}{ka_B} \quad , \quad (8)$$

with $a_B = \hbar^2/(Z\mu e^2)$ the Bohr radius. If $f(\theta)$ is defined to have the phase shifts $\sigma_l + \delta_l^{(sc)}$, with Coulomb-modified phase shifts $\delta_l^{(sc)}$ due to the short-ranged part of the interaction, then the partial-wave expansion of the Coulomb-modified scattering amplitude $f^{(sc)}(\theta)$ is given by

$$f^{(sc)}(\theta) = \frac{1}{k} \sum (2l+1) C_l^{(sc)} P_l(\cos\theta) \quad , \quad C_l^{(sc)} = e^{i\delta_l^{(sc)}} \sin\delta_l^{(sc)} \quad , \quad (9)$$

subject to the following partial-wave representation of the operator product $e^{2i\sigma} f^{(sc)}(\theta)$:

$$e^{2i\sigma} f^{(sc)}(\theta) = \frac{1}{k} \sum (2l+1) e^{2i\sigma_l} C_l^{(sc)} P_l(\cos\theta) \quad . \quad (10)$$

In practice, the Coulomb-modified partial wave amplitudes $C_l^{(sc)}$ are determined by solving the wave equation for each partial wave with point Coulomb boundary conditions at sufficiently large distance. The total reaction cross section is then given by

$$\sigma_R = \frac{4\pi}{k^2} \sum (2l+1) [\text{Im}C_l^{(sc)} - (\text{Im}C_l^{(sc)})^2 - (\text{Re}C_l^{(sc)})^2] \quad . \quad (11)$$

In addition to the \bar{p} reaction cross section, which near $E = 0$ is essentially exhausted by the total annihilation cross section, we also discuss in this paper the low energy effective-range expansion which requires the knowledge of the Coulomb-modified phase shifts $\delta_l^{(sc)}$. These are given in terms of the partial wave amplitudes as follows:

$$\text{Im}\delta_l^{(sc)} = -\frac{1}{4} \ln[(1 - 2\text{Im}C_l^{(sc)})^2 + 4(\text{Re}C_l^{(sc)})^2] \quad , \quad (12)$$

$$\cot(\text{Re}\delta_l^{(sc)}) = i \frac{[1 - 2\text{Im}C_l^{(sc)} + 2i\text{Re}C_l^{(sc)}]e^{2\text{Im}\delta_l^{(sc)}} + 1}{[1 - 2\text{Im}C_l^{(sc)} + 2i\text{Re}C_l^{(sc)}]e^{2\text{Im}\delta_l^{(sc)}} - 1} \quad , \quad (13)$$

where the latter expression is particularly useful in order to avoid a possible ambiguity in $\delta_l^{(sc)}$ if it is determined from an alternative expression involving $\sin(2\text{Re}\delta_l^{(sc)})$. We note that for absorptive potentials V_{opt} , the Coulomb-modified phase shifts are complex, with $\text{Im}\delta_l^{(sc)} \geq 0$. An alternative expression for σ_R in terms of transmission coefficients T_l is then given by

$$\sigma_R = \frac{\pi}{k^2} \sum (2l+1) T_l \quad , \quad T_l = 1 - e^{-4\text{Im}\delta_l^{(sc)}} \quad , \quad (14)$$

which explicitly shows that $\sigma_R=0$ for real potentials.

Finally, the low-energy effective-range expansion for $l = 0$, in the presence of an attractive Coulomb potential, is given by [11,12]:

$$C_0^2(\eta) k \cot \delta_0^{(sc)} - \frac{2}{a_B} h(\eta) = -\frac{1}{a_0^{(sc)}} + \frac{1}{2} r_0^{(sc)} k^2 + O(k^4) , \quad (15)$$

where

$$C_0^2(\eta) = \frac{2\pi\eta}{1 - e^{-2\pi\eta}} , \quad h(\eta) = \text{Re } \psi(i\eta) - \ln \eta , \quad (16)$$

and ψ is the digamma function [13]. For $\eta \gtrsim 1$, or equivalently $ka_B \lesssim 1$, the following limits hold:

$$C_0^2(\eta \gtrsim 1) \approx 2\pi\eta , \quad h(\eta) \approx \frac{1}{12\eta^2} + \frac{1}{120\eta^4} + \dots , \quad (17)$$

so that Eq. (15) for the effective range expansion reduces to

$$\frac{2\pi}{a_B} \cot \delta_0^{(sc)} \approx -\frac{1}{a_0^{(sc)}} + \frac{1}{2} \left(\frac{1}{3} a_B + r_0^{(sc)} \right) k^2 + O(k^4) . \quad (18)$$

In the present work we solve numerically the scattering wave equation down to $E_L = 100$ keV, where the linear dependence of the l.h.s. on k^2 is explicitly verified, in order to extract reliably the Coulomb modified low energy parameters. We recall, that in the absence of a Coulomb potential, the effective range expansion for a short-ranged potential (such as V_{opt}) assumes the form:

$$k \cot \delta_0 \approx -\frac{1}{a_0} + \frac{1}{2} r_0 k^2 + O(k^4) , \quad (19)$$

which can be derived from Eq. (15) upon taking the limit $\eta \rightarrow 0$. The Coulomb-modified scattering length $a_0^{(sc)}$ is related to the purely short-ranged scattering length a_0 by the following approximate expression [14,15]:

$$\frac{1}{a_0^{(sc)}} \approx \frac{1}{a_0} + \frac{2}{a_B} \left(\ln \frac{a_B}{2R} + 1 - 2\gamma \right) , \quad (20)$$

which assumes that $R \ll a_B$, where R is the range of the short-ranged potential and $\gamma = 0.5772\dots$ is the Euler constant.

III. THE ANTIPROTON-HYDROGEN SYSTEM

As a first step towards studying the \bar{p} -nucleus system we tried to fit the data for the \bar{p} hydrogen system with as simple an ‘optical potential’ \bar{v} as possible, choosing a Gaussian shape common to both real and imaginary parts. In the present application to the $\bar{p}p$ system the ‘density’ $\rho(r)$ in Eq. (3) was chosen as proportional to a Gaussian $\exp(-r^2/a_G^2)$ and normalized to a volume integral of 1. Total reaction cross sections were calculated at 6 momenta between 38 and 175 MeV/c [1,16] and the complex parameter b_0 was varied in

order to fit these recent low-energy data for a given value of a_G . This was repeated for several values of a_G between 1 and 2 fm. In all cases excellent fits to the annihilation cross sections were achieved, and consequently the range parameter a_G could not be determined uniquely from the annihilation cross sections. As we aim at using the same potential on both sides of the $E = 0$ borderline, we turned next to the $\bar{p}H$ atom. Using the same type of potential as above, excellent agreement between calculation and experiment [17,18] was achieved by varying b_0 for any value of a_G between 1 and 2 fm. However, requiring that both atomic and scattering data be described by the same potential \bar{v} , we find $a_G=1.5$ fm and $\bar{b}_0 = -0.15 + i1.8$ fm, leading to a combined χ^2 of 3.8 for the 6 data points for annihilation cross sections plus the 3 data points for the atom. The uncertainties are $\pm 0.15, \pm 0.15$ and ± 0.06 fm for a_G , $\text{Re } \bar{b}_0$ and $\text{Im } \bar{b}_0$, respectively. This potential will be referred to as potential (G). A more elaborate potential was previously shown [19,20] to be able to fit the low-energy $\bar{p}p$ annihilation data. In that potential the real part is described by a Saxon-Woods (SW) shape with a radius of 1.89 fm and diffuseness parameter of 0.2 fm whereas the imaginary part has the SW shape with a radius of only 0.41 fm and the same diffuseness of 0.2 fm. Adopting these geometries we repeated the procedure described above for fitting the annihilation and atomic data and obtained very good fits with a χ^2 of 5.8 for the 9 data points. The parameter \bar{b}_0 is $2.85 + i16.5$ fm, with about $\pm 10\%$ uncertainties, leading to potential depths of 46.5 and 7550 MeV for the real and imaginary parts, respectively, in very good agreement with Refs. [19,20]. This potential will be referred to as potential (SW). We note that for both potentials (G) and (SW), the imaginary part is considerably stronger than the real part, which signals a very strong absorptivity in the $\bar{p}p$ system. The real part of the potential, under such circumstances, plays only a minor role [4]. The imaginary parts of the potentials (G) and (SW) have markedly different ranges. The very short range of (SW) is qualitatively in agreement with other widely used phenomenological potentials [21,22], whereas the range of (G) is about twice as large as for these potentials.

Figure 1 shows results for the $\bar{p}p$ system. The upper part compares calculated reaction cross sections for the two potentials with the experimental values, and the excellent agreement is evident. The lower part shows the ratios of real to imaginary parts of the forward Coulomb-modified scattering amplitude $f^{(sc)}$ [see Eqs. (6) - (10)] for the two potentials, which is a quantity of considerable interest: this, so called ρ parameter, was determined at higher \bar{p} incident momenta to be positive, tending to zero between 200 - 300 MeV/c [23]. Our calculations give negative values for ρ at this lower-momentum range, indicating a smooth transition to the corresponding ratios for the Coulomb-modified scattering length also shown in the lower part, at zero energy, for potentials (G) and (SW). Evidently the two potentials, in spite of their different geometry, are very similar in predicting observable quantities.

IV. THE ANTIPROTON-NUCLEUS SYSTEM

With an established $\bar{p}p$ interaction potential \bar{v} , the simplest way of incorporating this potential into heavier \bar{p} -nuclear systems would be to fold it with the nuclear density to obtain a \bar{p} -nucleus potential: $V_{\text{opt}} = \bar{v} * \rho$. Setting aside possible renormalization effects in nuclei, this folding procedure also tacitly assumes that at low energy the spin-averaged $\bar{p}n$ interaction is approximately equal to the spin-averaged $\bar{p}p$ interaction, as supported by the

near equality of the imaginary parts of the corresponding scattering lengths [24] and also by several phenomenological $\bar{N}N$ potentials [21,22]. However, recent $\bar{n}p$ low-energy annihilation data from the OBELIX collaboration [25] suggest that the $\bar{n}p$ interaction, which by charge symmetry is equal to the $\bar{p}n$ interaction, is considerably weaker than the $\bar{p}p$ interaction. Therefore, we keep the strength of the density-folded \bar{p} -nucleus potential as a free parameter in our search, as is discussed below.

In the energy range covered by the present work the majority of data come from \bar{p} atoms and therefore this naive approach is best tested by applying the resulting potentials to \bar{p} atoms. We emphasize that the \bar{p} -nucleus potentials obtained from \bar{p} atoms are not unique. For ‘macroscopic’ nuclear densities of the type discussed in Ref. [8], and for $A > 10$, a Gaussian with a range parameter of about 1.5 fm leads to the best fit. Folding in the $\bar{p}p$ (G) potential with ‘macroscopic’ nuclear densities, we find that a *density-folded* optical potential of the form (3), with $b_0 = -0.1 + i1.2$ fm, fits all \bar{p} atoms heavier than boron ($A > 10$) with a χ^2 of 2.4 per point, whilst the corresponding value for a best-fit phenomenological potential of the form Eq. (3) using the same unfolded nuclear densities is 2.7 [8]. We denote this \bar{p} -nucleus density-folded optical potential by (F). The value of its strength parameter b_0 is 2/3 of the strength \bar{b}_0 of the $\bar{p}p$ potential (G). Note that this is not a best-fit potential but merely a renormalized $G * \rho$ potential, where a common factor is applied to the real and imaginary parts. Turning to $E > 0$, accurate experimental annihilation cross sections at low energies are scarce in this mass range, and we only note that the calculated cross sections for Ne are in reasonably good agreement with the data [3,26], as can be seen from Table I.

Having gained confidence in the applicability of the density-folded optical potential (F) for nuclei, we use it to calculate \bar{p} reaction cross sections over the periodic table for a range of energies, in order to study the systematics of the dependence on Z , on A and on the energy. Figure 2 shows, in the upper part, the calculated reaction cross sections for \bar{p} on Ne, Ca, Zr, Sn and Pb at 37.6, 57 and 106.6 MeV/c. It is seen that the range of values is very broad; for a given energy the calculated cross sections vary by a factor of between 6 and 10. For a given nucleus the cross sections vary with energy by a factor between 3.2 and 5.7. The mechanisms causing these variations are obviously of interest.

For strongly absorbed particles such as low energy antiprotons, disregarding the Coulomb potential, the total reaction cross section may be approximated by πR^2 where R is the radius of the nucleus. The underlying assumption is that antiprotons with impact parameter less than R , or equivalently with orbital angular momentum up to l_{\max} where semiclassically $l_{\max} + 1/2 = kR$, are totally absorbed. However, due to the focussing effect of the attractive Coulomb potential, particles with impact parameters larger than R also interact with the nucleus, thus causing the cross section to increase. The low energy Coulomb problem is well described by the semiclassical approach [10] as recognized a long time ago by Blair in connection with α particle reactions on nuclei [27]. Assuming that total absorption occurs in all partial waves for which the distance of closest approach is smaller than R , one gets the following relation between the Coulomb-modified l_{\max} and R :

$$(l_{\max} + \frac{1}{2})^2 \approx (kR)^2 \left(1 + \frac{2\eta}{kR}\right) . \quad (21)$$

At very low energies, $2\eta \gg kR$, and therefore $l_{\max} \gg kR$ due to the focussing effect of V_c . The total reaction cross section in the strong absorption limit is then given by

$$\sigma_R = \frac{\pi}{k^2} \sum (2l+1) \approx \frac{\pi}{k^2} (l_{\max} + \frac{1}{2})^2 \approx \pi R^2 (1 + \frac{2\eta}{kR}) = \pi R^2 (1 + \frac{2mZe^2}{\hbar^2 k_L k R}) , \quad (22)$$

where k_L and k are the laboratory and c.m. wave numbers, respectively. The second term within the brackets represents the Coulomb focusing effect and at very low energies it becomes dominant [4], thus leading to an $A^{1/3}Z$ dependence of the cross section if $R = r_0 A^{1/3}$. At high energies the usual strong absorption value πR^2 is obtained. In order to use this expression one needs to define an equivalent radius R that will properly represent the \bar{p} -nucleus interaction at the particular energy. We proceed to define such a radius.

Expanding the \bar{p} -nucleus scattering wave function in partial waves,

$$\psi(\mathbf{r}) = \sum (2l+1) \frac{\psi_l(r)}{r} P_l(\cos\theta) , \quad (23)$$

we define an average radius $\langle r_l \rangle$ for the l partial wave

$$\langle r_l \rangle = \frac{\int r W(r) |\psi_l(r)|^2 dr}{\int W(r) |\psi_l(r)|^2 dr} \quad (24)$$

with $W(r) = -\text{Im } V_{\text{opt}}(r)$. Then, bearing in mind the partial-wave expansion of the reaction cross section Eq. (14), we define an average radius as follows:

$$\langle r \rangle = \frac{\sum (2l+1) T_l \langle r_l \rangle}{\sum (2l+1) T_l} . \quad (25)$$

Expanding alternatively the reaction cross section Eq. (2) in partial waves:

$$\sigma_R = \frac{2}{\hbar v} \int W(r) 4\pi \sum (2l+1) |\psi_l(r)|^2 dr , \quad (26)$$

one finds that

$$T_l = \frac{8\mu k}{\hbar^2} \int W(r) |\psi_l(r)|^2 dr , \quad (27)$$

which combined with Eq. (25) leads to an equivalent expression for $\langle r \rangle$:

$$\langle r \rangle = \frac{\int W(r) |\psi(\mathbf{r})|^2 r d\mathbf{r}}{\int W(r) |\psi(\mathbf{r})|^2 d\mathbf{r}} . \quad (28)$$

Note that the average radius turns out to be slightly energy dependent. At $p_L = 37.6$ MeV/c, the lowest \bar{p} incident momentum for which $\bar{p}p$ annihilation has been measured [1], the calculated values of $\langle r \rangle$ appropriate to the density-folded optical potential (F) can be parameterized to better than 1% by

$$\langle r \rangle = 1.840 + 1.120 A^{1/3} \text{ fm} . \quad (29)$$

In fact, this expression holds to better than 2% for the whole range of very low energies up to $p_L \sim 100$ MeV/c.

In the lower part of Fig. 2 are plotted the ratios of the calculated cross sections to the semiclassical expression (22) where for R we took either the radius of a rigid sphere

having the same average radius as the optical potential (F), namely $R = \frac{4}{3} \langle r \rangle$, or just $R = \langle r \rangle$ which could be more appropriate due to the substantial attenuation of the wavefunction which is involved in the definition of $\langle r \rangle$. It is seen that these ratios vary remarkably little, by less than 5% for the lower band, when the cross sections vary by factors between 3 and 10. At the lower energy the Coulomb focusing is dominant but at the higher energies covered here both terms of Eq. (22) are important. It may therefore be concluded that the dependence of the calculated reaction cross sections on the three parameters (Z , A and energy) is almost exclusively given by Eq. (22).

Another consequence of the strongly absorptive \bar{p} -nucleus optical potential is the saturation of the physical observables which are induced by the absorptivity. Thus, for $E < 0$, widths of \bar{p} atomic levels saturate as function of the magnitude of $\text{Im } V_{\text{opt}}$ [5,6] and, for $E > 0$, total reaction cross sections also saturate with it [4]. As argued in our earlier work [4], the saturation property of σ_R for any given nucleus also implies that σ_R does not rise with Z and A as fast as it would have risen if the \bar{p} absorption were considerably weaker and therefore could be treated perturbatively. This is demonstrated here differently, in Fig. 3, where the saturation factor S defined as

$$S = \frac{\sigma_R(\text{Im} b_0)/\text{Im} b_0}{\sigma_R(10^{-4}\text{Im} b_0)/10^{-4}\text{Im} b_0} \quad (30)$$

is plotted at $p_L = 57$ MeV/c (1.73 MeV) as function of A , using the density-folded optical potential (F) for $A > 10$, (F') for ${}^4\text{He}$ (see below in Sect. V) and (G) for H. For $\text{Im } b_0$ as small as 10^{-4} of its nominal value (of 1.2 fm for potential (F)), the calculated σ_R is very nearly linear in $\text{Im } b_0$. If the linear rise of σ_R were sustained up to the nominal value, the saturation factor S would have assumed the value $S = 1$. However, for $\text{Im } b_0 = 1.2$ fm for potential (F), the calculation is strongly nonperturbative, as witnessed in the figure by the small values of S relative to 1, about 0.1 and less beginning with Ne. The saturation of σ_R has two aspects to it: (i) that S depends very weakly on $\text{Im } b_0$ in the nonperturbative regime (not shown in the figure); and (ii) that S monotonically decreases with A , as is shown in the figure, both for antiprotons (solid curve) and for antineutrons (dashed curve). The values of S for antiprotons are lower than for antineutrons due to the Coulomb focussing effect which for antiprotons acts in two seemingly opposing ways: (i) enhancing the reaction cross section in the negatively charged case compared to the uncharged case, but also (ii) expelling more effectively [5,6] the \bar{p} wavefunction from the nuclear region, so that σ_R becomes more strongly suppressed than for antineutrons. This latter effect gets weaker with increasing energy; at $E_L = 6.04$ MeV, $S_{\bar{p}}$ is larger by 20 - 25 % than at 1.73 MeV, whereas $S_{\bar{n}}$ is smaller than at 1.73 MeV.

V. THE ANTIPIRON - HELIUM SYSTEM

In this section we study the $\bar{p} - {}^{3,4}\text{He}$ system at very low energies, within the optical model approach, in order to test the scattering-length approximation (SLA) which was successfully applied to the $\bar{p}p$ system [28] and has recently been extended to the $\bar{p}d$ and $\bar{p} - {}^4\text{He}$ systems [7]. ${}^4\text{He}$ is one of the very few nuclei for which data on the strong interaction of \bar{p} are available for both the very low energy scattering regime and the atomic negative energy regime. There are two data points for the total annihilation cross section below 3 MeV in

the positive energy regime [2], and three data points for the atomic $2p$ level shift and width plus the width of the $3d$ level [29] above -20 keV in the negative energy regime. We chose to test the ability of the optical model to reproduce these data together with the corresponding set of atomic shift and widths data for ^3He [29], although the optical model approach is not very well suited for studying such light nuclear targets.

Since potential (F) does not reproduce very well the \bar{p} -nuclear observables for $A < 10$, we searched over its parameters to fit the \bar{p} - ${}^{3,4}\text{He}$ data mentioned above. As was already encountered in the fitting procedure described in our earlier work [4] for potential (a) of that reference, when trying to fit the atomic $2p$ and $3d$ levels simultaneously the calculated width of the $2p$ state in ${}^4\text{He}$ came out too small. This has been noted by other researchers before, as summarized in Ref. [29]. We therefore dropped out the $3d$ widths data from the fitting procedure, partly on the grounds that the d -wave contribution to the very low energy \bar{p} annihilation cross sections, which are also being explored here, is almost negligible compared to the dominant s and p waves (see below). The resulting density-folded optical potential, referred to as (F'), has the following parameters: $a_G = 1.8$ fm for the range parameter of the two-body Gaussian interaction folded in with the He densities, and a strength parameter $b_0 = -0.26 + i2.07$ fm in the notation of Eq. (3). The optical potential (F') is more absorptive than potential (F) and, again, its real part plays only a minor role. The $2p$ level shifts and widths, as well as the \bar{p} total annihilation cross sections calculated using the optical potential (F') are shown in Table II, where the measured values are also given, including a recent report of \bar{p} annihilation on ${}^3\text{He}$ [30]. Clearly, potential (F') describes well these data. We note that omitting the ${}^3\text{He}$ data from the fit hardly changes the resultant (F') which describes very well the ${}^4\text{He}$ data. In particular, it was not possible to decrease, within such a restricted fit, the range parameter a_G from its relatively large value given above.

Protasov et al. [7] have recently fitted the two low-energy \bar{p} - ${}^4\text{He}$ total annihilation cross sections listed in the table, using the SLA expressions for s , p and d waves [28]. The input p - and d -wave Coulomb-modified scattering ‘lengths’ were derived using the Trueman formula [12] from the $2p$ shift and $2p$ and $3d$ widths. The s -wave Coulomb-modified scattering length $a_0^{(sc)}$ was left as a fitting parameter, since the \bar{p} atomic $1s$ level shift and width in He are not known experimentally. Assuming a value of 1.0 ± 0.5 fm for $\text{Re } a_0^{(sc)}$, these authors were able to fit the annihilation cross sections with the following value for the imaginary part of the s -wave Coulomb modified scattering length:

$$\text{Im } a_0^{(sc)} = -0.36 \pm 0.03(\text{stat.})^{+0.19}_{-0.11}(\text{syst.}) \text{ fm} . \quad (31)$$

The quality of the fit, as is evident from Fig. 3 in Ref. [7], is similar to ours (see Table II above), with the calculated lower (higher) energy cross section somewhat above (below) the mean value of the measurement. In contrast, our \bar{p} - ${}^4\text{He}$ potential (F'), which is also fitted to essentially the same data set, upon using Eq. (18) yields the following values:

$$\text{Re } a_0^{(sc)} = 1.851 \text{ fm} , \quad \text{Im } a_0^{(sc)} = -0.630 \text{ fm} . \quad (32)$$

It is clear from this example that the ‘model independent’ determination claimed by Protasov et al. for $a_0^{(sc)}$ is violated by our specific example, suggesting that, contrary to their claim, it is not a model independent determination. In order to study the origin of the above

discrepancy, we show in Table III the partial wave contributions to the calculated cross section at $p_L = 57$ MeV/c. The most important contributions are due to the s - and p -waves, for which the two calculations give quite different results in spite of agreeing well with respect to their sum. In particular, the p -wave contributions are quite different from each other, although sharing practically the *same* value of the Coulomb-modified p -wave ‘scattering length’ (more traditionally called ‘scattering volume’) $a_1^{(sc)}$. Whereas at -20 keV, the $l = 1$ \bar{p} - ${}^4\text{He}$ dynamics is well determined by $a_1^{(sc)}$ alone, over the energy range of 1 - 3 MeV corresponding to the annihilation measurements, it depends on more than just this ‘scattering length’. The effective range term, and perhaps higher order terms in the effective range expansion at low energies, become equally important. Indeed, we have verified for potential (F') that the variation of the Coulomb-modified $l = 1$ scattering phase shift is not reproduced in this energy range by specifying the ‘scattering length’ alone. Once the p -wave contributions to the total annihilation cross section differ by as much as is observed in the table, the essentially fitted s -wave contribution in the calculation of Ref. [7] must also differ, and hence our prediction for the Coulomb-modified s -wave scattering length is necessarily different from that of Ref. [7]. Such a difference would not occur for the $\bar{p}p$ system, which at the appropriate low energies is largely controlled by s waves [28].

Protasov et al. [7] also attached particular significance to the observation that, for the Coulomb-modified s -wave scattering length, “the absolute value of the scattering length seems to be a decreasing function of the atomic weight” since “a naive geometrical picture of \bar{p} -nucleus annihilation would suggest a value of the \bar{p} -nucleus scattering length increasing with the nuclear size.” Indeed, their expectation holds for the plain strong-interaction (not the Coulomb-modified) scattering lengths, as borne out by the calculations of Ref. [31] which are updated in the next Section VI. However, the Coulomb-modified scattering lengths do not show such a clear geometrical picture, as is also discussed in Section VI.

VI. ANTIPROTON - NUCLEUS SCATTERING LENGTHS

In an earlier paper [31], hadron nucleus scattering lengths were derived from exotic atom data for kaons, antiprotons and sigma hyperons. For the purposes of the present paper, we have updated the previous calculations for antiprotons, using more recent experimental measurements of strong interaction shifts and widths.

For exotic atoms with $Z > 1$, strong interaction measurements are only available for angular momentum states with $l > 0$. As a result it is necessary to use an optical model approach as an intermediate step in deriving the s -wave Coulomb-modified scattering length $a_0^{(sc)}$, or the purely strong-interaction scattering length a_0 from the measured strong interaction effects for $l > 0$ atomic states. In this method, the optical potential given by Eq. (3) was used to fit the strong interaction shift and width values for individual nuclei by adjusting the real and imaginary parts of the optical strength parameter b_0 . The s -wave scattering length a_0 was then calculated by solving the Klein-Gordon equation for $l = 0$ with the optical potential V_{opt} , but without the Coulomb potential, at an energy (1 keV) close to threshold. Further details of the method are given in the earlier paper [31].

The experimental shift and width measurements were taken from the published literature and cover the available target elements from C to Pr inclusive, omitting Yb since the nucleus is deformed. The data set used is discussed and tabulated in [8,32]. For the present work,

single particle distributions were used [8,32] for $\rho(r)$ as these are expected to be more appropriate for the analysis of antiproton data. In the previous analysis [31], macroscopic density distributions were used.

The results of the present analysis are shown in Fig. 4 and are qualitatively similar to those obtained earlier [31], where an opposite sign convention was used for a_0 (there denoted a_s). Again the real part of the scattering length shows an approximate $A^{1/3}$ dependence, and the imaginary part is constant. This is to be expected on the basis of a simple model based on a strongly absorbing square well potential [31]. A least squares fit to these scattering length values gives:

$$\text{Re } a_0 = (1.54 \pm 0.03) A^{0.311 \pm 0.005} \text{ fm}, \quad \text{Im } a_0 = -1.00 \pm 0.04 \text{ fm} \quad . \quad (33)$$

These best fit parameter values are in excellent agreement with those obtained earlier [31]. We note that the magnitude of $\text{Im } a_0$ is considerably larger than expected for a sharp-edge potential, resulting mainly from the diffuseness of the potential [31,33].

For completeness, values for a_0 for nuclei with $A < 10$ are also shown in Fig. 4. The values for ^6Li and ^7Li were determined using the method described above from the strong interaction shift and width measurements of Poth et al. [34]. The values for ^3He and ^4He were calculated using potential (F') described in Sect. V. The value for hydrogen was obtained with potential (G) described in Sect. III. The real parts of a_0 for these light nuclei are seen to deviate from the predictions of the best fit parameters for $A > 10$ described earlier, whilst the imaginary parts remain relatively independent of A .

To confirm this behaviour for nuclei with $A < 10$, the analysis of the strong interaction data for C to Pr [8,32], together with that for ^6Li and ^7Li [34], was repeated fitting all the data simultaneously with a single value for the complex parameter b_0 . A good fit to the strong interaction data is obtained with a χ^2 of 52 for 46 data points. The s -wave scattering lengths obtained in this way are typically a factor of 5 more precise than those in Fig. 4, which were obtained using fits to individual nuclei, but they are model dependent since it is assumed that the data for all nuclei can be fitted with a single value of b_0 . However this seems to be a reasonable assumption in view of the very good fit to the data. The results confirm the deviation in the value of $\text{Re } a_0$ for ^6Li and ^7Li from the simple parameterization for $A > 10$ nuclei shown in Fig. 4(top). The absolute values of $\text{Im } a_0$ of 1.27 ± 0.04 and 1.16 ± 0.04 fm for ^6Li and ^7Li respectively, are larger than the mean absolute value of $\text{Im } a_0 = 1.04 \pm 0.01$ fm obtained for $A > 10$.

To conclude this section, we wish to study the A dependence of the \bar{p} -nucleus Coulomb-modified s -wave scattering length $a_0^{(sc)}$ for a *given* potential, here chosen as potential (F). The calculated values of $a_0^{(sc)}$ for light and medium-weight nuclei are given in the first two rows of Table IV. The behaviour of these scattering lengths with A does not follow a clear geometrical picture. The real part at first increases, it then decreases very quickly and flips sign, becoming negative already for ^{12}C . Another sign flip occurs somewhere between Ne and Ca. This oscillatory behaviour of $\text{Re } a_0^{(sc)}$ is very different from the smooth rise of $\text{Re } a_0$ with A (Eq. (33) and Fig. 4). The magnitude of the imaginary part at first increases with A (rather than decreasing according to the speculation of Ref. [7]), reaching a maximum value somewhere near $A \sim 11 - 12$ approximately where $\text{Re } a_0^{(sc)}$ vanishes, it then decreases to a minimum value somewhere between Ne and Ca. This behaviour of $\text{Im } a_0^{(sc)}$ is very different from the approximate constancy established above for $\text{Im } a_0$.

The behaviour of $a_0^{(sc)}$ as function of A can be qualitatively understood using the approximate relation Eq. (20) between a_0 and $a_0^{(sc)}$ which assumes that $R \ll a_B$, where R is the range of the short-ranged potential giving rise to a_0 , and a_B is the Bohr radius. Neglecting $(\text{Im } a_0)^2$ relative to $(\text{Re } a_0)^2$, approximating R by $\text{Re } a_0 \approx 1.5A^{1/3}$ fm and keeping only the logarithmic term within the brackets in Eq. (20), the condition for $\text{Re } a_0^{(sc)} = 0$ is given by $\ln t \approx -t$, where $t = a_B^{(p)}/(3A^{4/3})$ with $a_B^{(p)} = 57.64$ fm for the Bohr radius of $\bar{p}p$ and assuming $Z = A/2$. This condition is satisfied for $A \approx 14$ for which $R = 3.62$ fm according to the above approximations, so that the condition of applicability $R \ll a_B = 4.41$ fm is still (although barely) satisfied. Relaxing the numerically unnecessary approximations of neglecting $\text{Im } a_0$ and $(1 - 2\gamma)$, the vanishing of $\text{Re } a_0^{(sc)}$ occurs for $A \approx 13.5$, where $\text{Im } a_0^{(sc)}$ attains a substantial maximum. Thus, Eq. (20) explains well, within its limited range of validity, the main features of $\text{Re } a_0^{(sc)}$ and $\text{Im } a_0^{(sc)}$ from Table IV. The ‘non-geometric’ dependence of $a_0^{(sc)}$ on A is due to the logarithmic term in Eq. (20) which arises from the unavoidable logarithmic behaviour of the Coulomb wavefunctions [10].

The s -wave Coulomb-modified scattering lengths $a_0^{(sc)}$ correspond to the short-ranged potential which, strictly speaking, is superposed on a *point* Coulomb potential $V_c^{(\text{point})} = -Z\alpha/r$. This short-ranged potential consists then, in addition to the strong-interaction optical potential V_{opt} , of the short-ranged Coulomb term $V_c(r) - V_c^{(\text{point})}(r)$. In practice we have also included a vacuum-polarization potential in the latter short-ranged contribution. The Coulomb-modified phase shifts $\delta_l^{(sc)}$ due to the short-ranged part of the interaction, and the related scattering ‘lengths’ $a_l^{(sc)}$ considered in Sect. II, therefore include also effects which are not entirely due to the strong interactions. To be more precise, the superscript (sc) should be replaced by $(st + fs; pc)$, that is *strong + finite size* with respect to *point Coulomb*. It would be more fitting, perhaps, to define the Coulomb-modified phase shifts $\delta_l^{(st; fs+pc)}$, due exclusively to the strong interactions with respect to the overall Coulomb potential V_c . Similarly, one could also define the ‘finite-size’ Coulomb-modified phase shifts $\delta_l^{(fs; pc)}$ due to the short-ranged non strong-interaction potential with respect to $V_c^{(\text{point})}$. It is straightforward to show that

$$\delta_l^{(sc)} \equiv \delta_l^{(st+fs;pc)} = \delta_l^{(st;fs+pc)} + \delta_l^{(fs;pc)} . \quad (34)$$

Using Eq. (18) and similarly tailored low-energy effective-range expansions, Eq. (34) leads to the following relation between the corresponding scattering lengths:

$$\tilde{a}_0^{(sc)} \equiv a_0^{(st;fs+pc)} = \frac{a_0^{(sc)} - a_0^{(fs;pc)}}{1 + (2\pi/a_B)^2 a_0^{(sc)} a_0^{(fs;pc)}} , \quad (35)$$

where $a_0^{(sc)} \equiv a_0^{(st+fs;pc)}$ is the same Coulomb-modified short-ranged scattering length hitherto considered and tabulated in the first two rows of Table IV, $a_0^{(fs;pc)}$ is due to the finite size Coulomb (plus vacuum polarization) effect, and $\tilde{a}_0^{(sc)} \equiv a_0^{(st;fs+pc)}$ on the l.h.s. is the intrinsically strong-interaction Coulomb modified scattering length. We have also tabulated these newly defined scattering lengths in Table IV. The real finite size scattering length $a_0^{(fs;pc)}$ rises modestly with Z , becoming significant for ^{12}C where it leads to a change from -0.6 fm for $\text{Re } a_0^{(sc)}$ to 0.9 fm for $\text{Re } \tilde{a}_0^{(sc)}$. The induced change for $\text{Im } a_0^{(sc)}$ into $\text{Im } \tilde{a}_0^{(sc)}$ already becomes significant for ^9Be . However, the general trend of $\tilde{a}_0^{(sc)}$ with A is qualitatively similar to that described and discussed earlier for $a_0^{(sc)}$.

VII. SUMMARY AND CONCLUSIONS

We have shown in this work that a unified optical-model description of low-energy antiproton interactions can be successfully achieved using a density-folded \bar{p} optical potential $V_{\text{opt}} \sim \bar{v} * \rho$. As shown in Sect. III, the potential \bar{v} gives an excellent fit to the measured $\bar{p}p$ annihilation cross sections at low energies ($p_L < 200$ MeV/c) and to the $1s$ and $2p$ spin-averaged $\bar{p}H$ level shifts and widths, but is far from being unique; other combinations of range and of strength parameters have been derived for the $\bar{p}p$ system for low as well as for higher energies [19,20], all of which yield a highly absorptive potential. It would be useful to measure also $\bar{p}p$ elastic scattering differential cross sections at these low energies, including the Coulomb-nuclear interference angular region, in order to attempt resolving the ambiguity in the determination of \bar{v} , particularly its less well determined real part.

The optical potential V_{opt} reproduces satisfactorily the \bar{p} atomic level shifts and widths across the periodic table for $A > 10$ as well as the few annihilation cross sections measured on Ne. This simple folding model does not work well for the very light species of He and Li, possibly due to the spin and isospin averaging and to other unjustified approximations inherent in the construction of optical potentials for these relatively small values of A . However, for a limited range of small- A values, as shown in Sect. V for the He isotopes, an energy-independent optical potential can be fitted to both the measured annihilation cross sections at $E > 0$ and the atomic shift and width data for $E < 0$. Our detailed analysis of the $\bar{p}-^4\text{He}$ system was primarily intended to demonstrate the inapplicability of treating it by the scattering length approximation [7]. As a byproduct, we have discussed in Sect. VI the systematics of several sets of \bar{p} - nucleus s -wave scattering lengths, the purely strong-interaction set for which we confirmed and updated the discussion of Ref. [31], and the Coulomb-modified set which defies any geometrical interpretation.

Fairly accurate reproduction of the optical potential calculations of σ_R was achieved in Sect. IV by extending the black-disk strong-absorption model [27] to account for the Coulomb focussing effect of negatively charged projectiles at very low energies ($p_L < 100$ MeV/c). As the number of additional partial waves contributing to the \bar{p} reaction cross section due to the Coulomb focusing effect increases substantially upon decreasing the incoming energy, the semiclassical description becomes valid, resulting in the simple closed-form ‘geometrical’ expression (22) which embodies the overall dependence of σ_R on Z , A and on E , provided the black-disk radius is properly handled (see Eq. (29)). Figure 2(bottom) demonstrates this success for very low \bar{p} energies over the periodic table.

A final comment is due to the apparent success of using a density folded optical potential in terms of a potential \bar{v} that describes well the $\bar{p}p$ system. Deloff and Law advocated and used a $\bar{v} * \rho$ folding model for kaonic atoms [35,36] and for \bar{p} atoms [37]. This model was subsequently tested by Batty for kaonic atoms [38] and for antiprotonic and sigma atoms [39], and moderately good agreement with the data was found. However, the underlying potentials \bar{v} were not fitted to a comprehensive set of $Z = 1$ data. The present work provides a step forward for antiprotons, in that a complete body of $\bar{p}p$ data was fitted to determine \bar{v} . This has to be supplemented in due course by $\bar{p}n$ data, particularly in order to understand the renormalization factor of 2/3 encountered in obtaining the density-folded optical potential (F) from the \bar{v} potential (G). A multiple-scattering justification of the $\bar{v} * \rho$ folding model was given by Green and Wycech [40] for antiprotons as due to the strong

absorptivity, and was confirmed in detailed calculations by other authors [41,42].

Clearly, more data on \bar{p} nuclear interactions at low energies are needed to develop quantitatively further the unified optical-model approach put forward in the present work. Such data should consist of elastic and charge exchange scattering, as well as annihilation cross sections on nuclei. In particular, data on the very light nuclei, for $A < 10$, would provide valuable information on how to bridge the gap, prevailing at present within the density-folded optical model approach, between hydrogen and the $A > 10$ nuclei concerning the applicability of the same (smoothly dependent on A) \bar{p} optical potential.

CJB wishes to thank the Hebrew University for support for a visit during which this work was started.

This research was partially supported by the Israel Science Foundation.

REFERENCES

- [1] A. Zenoni et al., Phys. Lett. B 461 (1999) 405.
- [2] A. Zenoni et al., Phys. Lett. B 461 (1999) 413.
- [3] A. Bianconi et al., Phys. Lett. B 481 (2000) 194.
- [4] A. Gal, E. Friedman, C.J. Batty, Phys. Lett. B 491 (2000) 219.
- [5] E. Friedman, A. Gal, Phys. Lett. B 459 (1999) 43.
- [6] E. Friedman, A. Gal, Nucl. Phys. A 658 (1999) 345.
- [7] K.V. Protasov, G. Bonomi, E. Lodi Rizzini, A. Zenoni, Eur. Phys. J. A 7 (2000) 429.
- [8] C.J. Batty, E. Friedman, A. Gal, Phys. Rep. 287 (1997) 385.
- [9] E. Friedman, A. Gal, J. Mareš, Nucl. Phys. A 625 (1997) 272.
- [10] L.I. Schiff, Quantum Mechanics, third edition (McGraw Hill, New York, 1968).
- [11] H.A. Bethe, Phys. Rev. 76 (1949) 38.
- [12] T.L. Trueman, Nucl. Phys. 26 (1961) 57.
- [13] M. Abramowitz, I.A. Stegun, Handbook of Mathematical Functions (Dover, New York, 1965).
- [14] J.D. Jackson, J.M. Blatt, Rev. Mod. Phys. 22 (1950) 77.
- [15] B.R. Holstein, Phys. Rev. D 60 (1999) 114030.
- [16] A. Bertin et al., Phys. Lett. B 369 (1996) 77.
- [17] M. Augsburger et al., Nucl. Phys. A 658 (1999) 149.
- [18] D. Gotta et al., Nucl. Phys. A 660 (1999) 283.
- [19] W. Brückner et al., Phys. Lett. B 166 (1986) 113.
- [20] A. Bianconi et al., Phys. Lett. B 483 (2000) 353.
- [21] C.B. Dover, J.M. Richard, Phys. Rev. C 21 (1980) 1466; J.M. Richard, M.E. Sainio, Phys. Lett. B 110 (1982) 349.
- [22] M. Kohno, W. Weise, Nucl. Phys. A 454 (1986) 429.
- [23] W. Brückner et al., Phys. Lett. B 158 (1985) 180.
- [24] G.S. Mutchler et al., Phys. Rev. D 38 (1988) 742.
- [25] A. Bertin et al., Nucl. Phys. B (Proc. Suppl.) 56A (1997) 227.
- [26] F. Balestra et al., Nucl. Phys. A 452 (1986) 573.
- [27] J.S. Blair, Phys. Rev. 95 (1954) 1218.
- [28] J. Carbonell, K.V. Protasov, A. Zenoni, Phys. Lett. B 397 (1997) 345.
- [29] M. Schneider et al., Z. Phys. A 338 (1991) 217.
- [30] A. Bianconi et al., Phys. Lett. B 492 (2000) 254.
- [31] C.J. Batty, Nucl. Phys. A 411 (1983) 399.
- [32] C.J. Batty, E. Friedman, A. Gal, Nucl. Phys. A 592 (1995) 487.
- [33] V.A. Karmanov, K.V. Protasov, A.Yu. Voronin, Eur. Phys. J. A 8 (2000) 429.
- [34] H. Poth et al., Nucl. Phys. A 466 (1987) 667.
- [35] A. Deloff, J. Law, Phys. Rev. C 10 (1974) 1688.
- [36] A. Deloff, Phys. Rev. C 21 (1980) 1516.
- [37] A. Deloff, J. Law, Phys. Rev. C 10 (1974) 2657.
- [38] C.J. Batty, Nucl. Phys. A 372 (1981) 418.
- [39] C.J. Batty, Nucl. Phys. A 372 (1981) 433.
- [40] A.M. Green, S. Wycech, Nucl. Phys. A 377 (1982) 441.
- [41] T. Suzuki, H. Narumi, Nucl. Phys. A 426 (1984) 413.
- [42] J. Kronenfeld, A. Gal, J.M. Eisenberg, Nucl. Phys. A 430 (1984) 525.

FIGURES

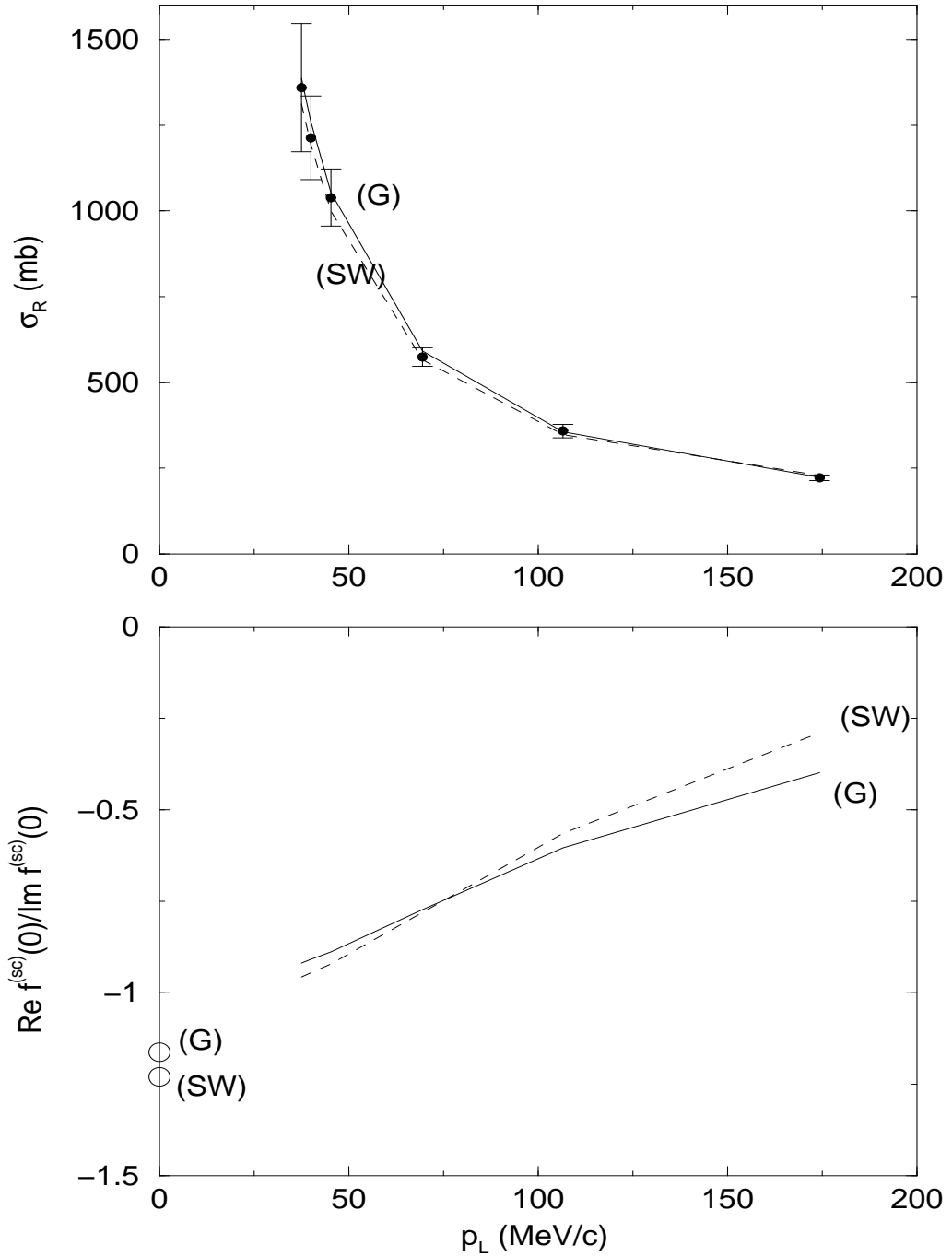


FIG. 1. Top: experimental annihilation cross sections [1,16] for the $\bar{p}p$ system and calculated values using the (G) and (SW) potentials. Bottom: ratios of the real part of the $\bar{p}p$ Coulomb-modified forward scattering amplitude to its imaginary part for the same potentials. Real to imaginary ratios for the zero-energy scattering length are also shown.

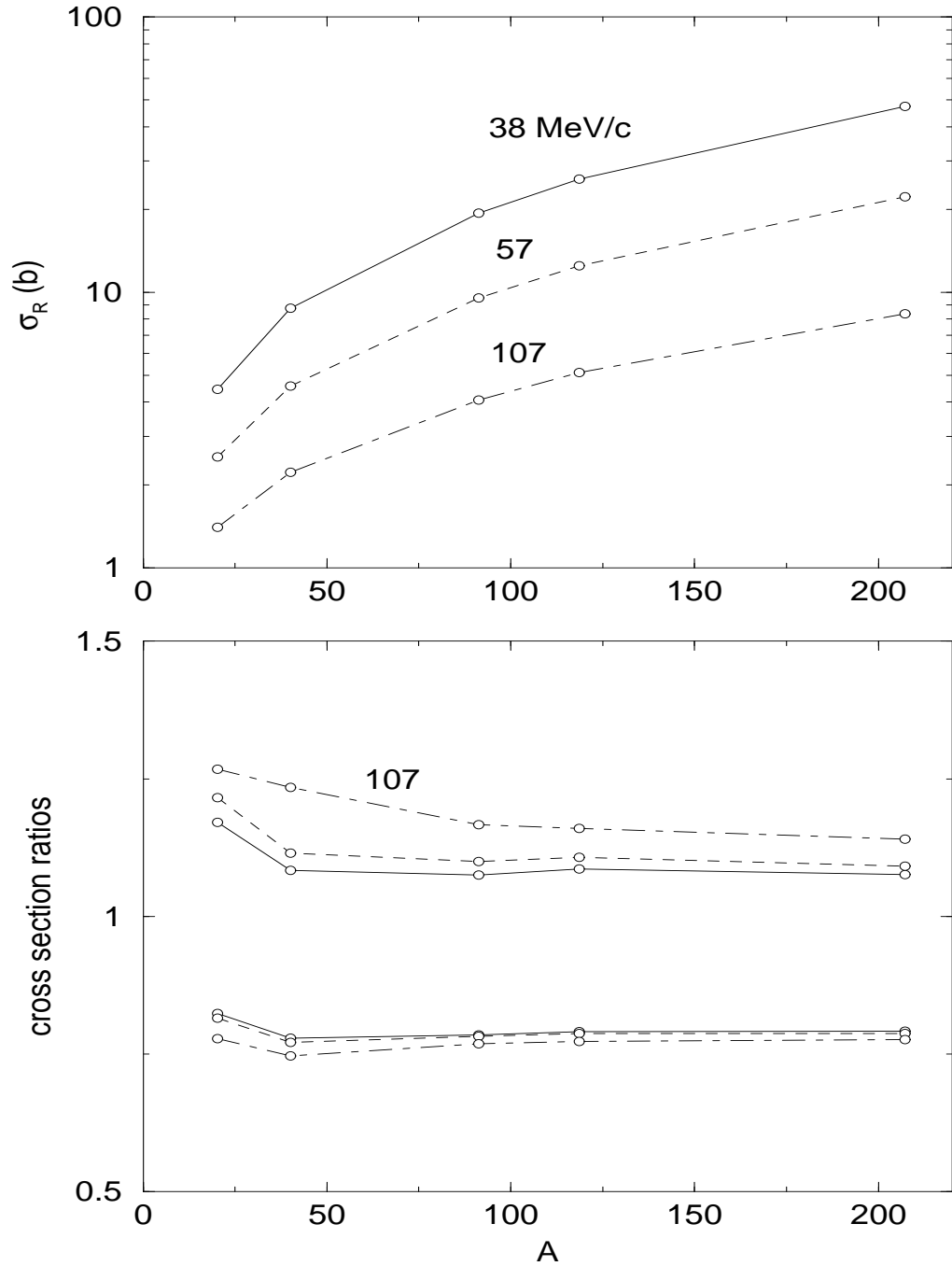


FIG. 2. Top: calculated \bar{p} -nucleus reaction cross sections for three incoming momenta using the density-folded potential (F). Bottom: ratios of the above cross sections to the semiclassical expression Eq. (22). Upper band for $R = \langle r \rangle$, lower band for $R = \frac{4}{3} \langle r \rangle$.

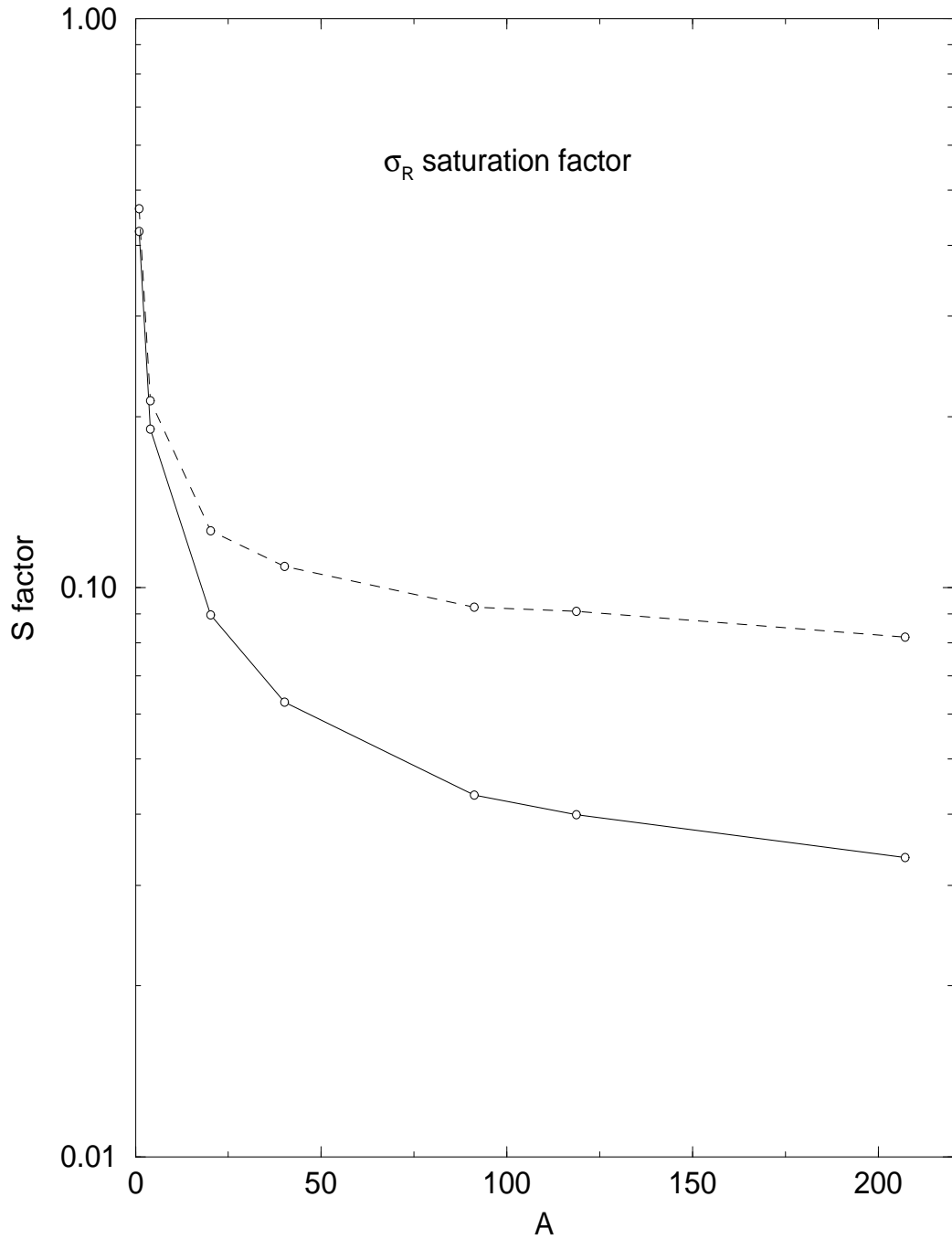


FIG. 3. The saturation factor S of Eq. (30) at $p_L = 57$ MeV/c, calculated using the density-folded optical potential (F) for $A > 10$, (F') for $A = 4$ and (G) for $A = 1$, as function of A for antiprotons (solid line) and for antineutrons (dashed line).

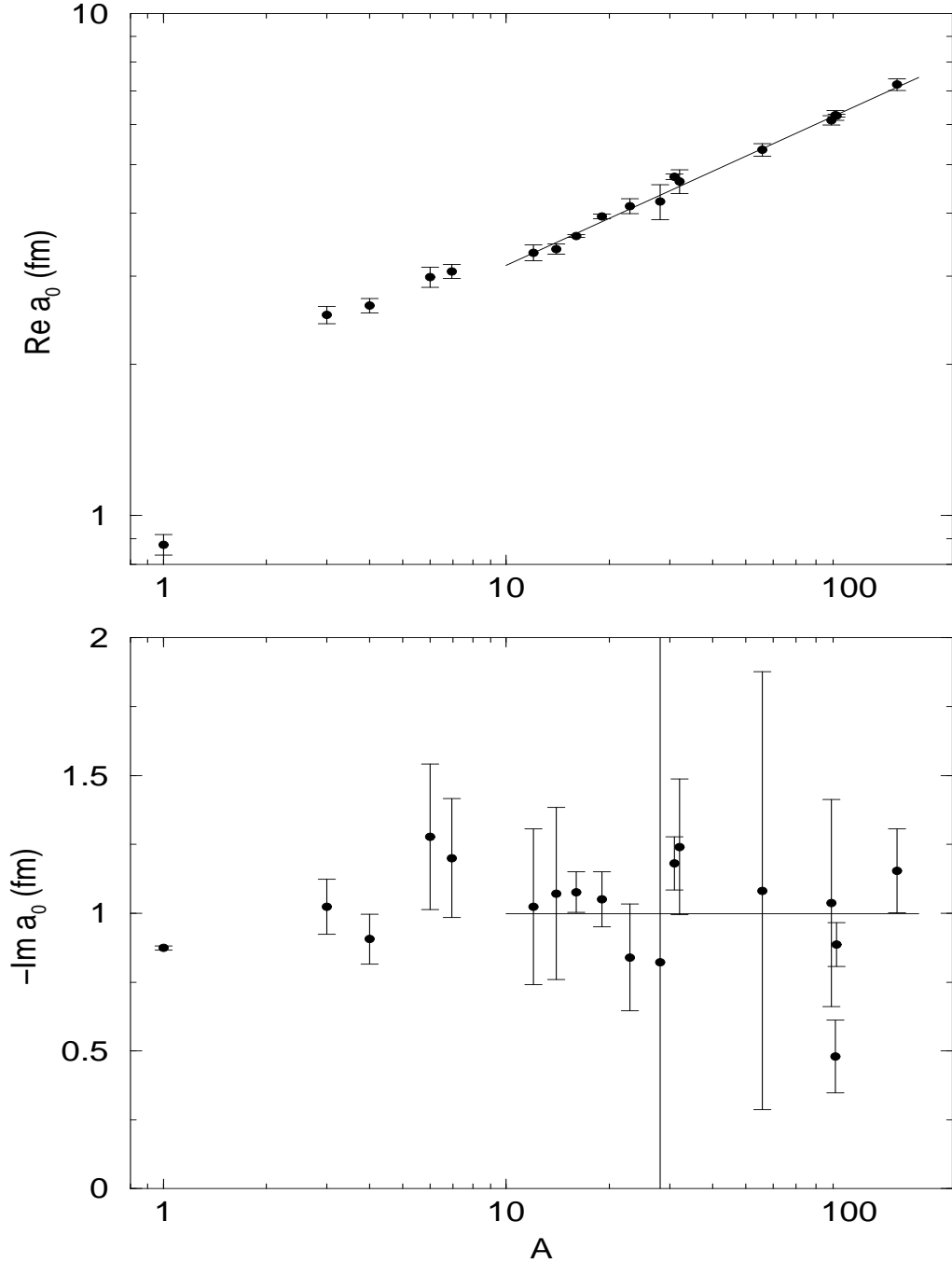


FIG. 4. Real (top) and Imaginary (bottom) parts of the s -wave \bar{p} scattering length a_0 calculated by fitting to \bar{p} atomic data. The straight lines are a best fit to the calculated values for $A > 10$, see Eq. (33).

TABLES

TABLE I. Measured and calculated annihilation cross sections for \bar{p} on Ne. Calculations were made with potential (F).

p_L (MeV/c)	$\sigma_{ann}^{(exp)}$ (mb)	$\sigma_{ann}^{(calc)}$ (mb)
57	2210 ± 1105^a	2524
192.8	956 ± 47^b	1016

^a Ref. [3]

^b Ref. [26]

TABLE II. Measured and calculated observables for the $\bar{p}-{}^3,{}^4\text{He}$ system. Shifts (ε) and widths (Γ) are in eV, cross sections are in mb. Calculations were made with potential (F').

	ε_{2p}	Γ_{2p}	σ_{ann} (47.0 MeV/c)	σ_{ann} (55.0 MeV/c)	σ_{ann} (70.4 MeV/c)
${}^3\text{He}$ calc.	-12	33	—	1038	—
${}^3\text{He}$ exp.	-17 ± 4^a	25 ± 9^a	—	1850 ± 700^c	—
${}^4\text{He}$ calc.	-19	42	1116	—	810
${}^4\text{He}$ exp.	-18 ± 2^a	45 ± 5^a	979 ± 145^b	—	827 ± 38^b

^a Ref. [29]

^b Ref. [2]

^c Ref. [30]

TABLE III. Partial wave contributions (in mb) to the calculated \bar{p} - ${}^4\text{He}$ total annihilation cross section at $p_L = 57$ MeV/c.

	$l = 0$	$l = 1$	$l = 2$	$l = 3$	sum
Protasov et al. ^a	280.3	652.5	16.2		949
potential (F')	395.8	500.3	49.8	1.5	949
experiment ^b					915 ± 32

^a Ref. [7]

^b Ref. [3]

TABLE IV. Coulomb-modified s -wave \bar{p} scattering lengths (in fm) calculated for potential (F).

target	${}^4\text{He}$	${}^6\text{Li}$	${}^9\text{Be}$	${}^{10}\text{B}$	${}^{12}\text{C}$	${}^{16}\text{O}$	Ne	Ca
$\text{Re } a_0^{(sc)}$	1.562	1.967	2.169	1.401	-0.626	-0.645	-0.216	0.134
$\text{Im } a_0^{(sc)}$	-0.590	-1.012	-1.792	-2.853	-2.631	-0.551	-0.241	-0.391
$a_0^{(fs;pc)}$	0.067	0.148	0.170	0.183	0.176	0.252	0.307	0.835
$\text{Re } \tilde{a}_0^{(sc)}$	1.479	1.703	1.809	1.633	0.948	-0.654	-0.485	0.004
$\text{Im } \tilde{a}_0^{(sc)}$	-0.576	-0.853	-1.183	-1.612	-2.373	-1.414	-0.556	-0.121